Journal of ELECTRONIC MATERIALS, Vol. 50, No. 6, 2021
https://doi.org/10.1007/s11664-021-08869-w

ORIGINAL RESEARCH ARTICLE

Methane Sensitivity of Alpha-Fe_2O_3 Obtained from Pechini Combustion Synthesis using Different Organic Fuels

INDRANIL DAS,[1] ANUPAM NANDI,[1] RITTWIK MAJUMDER,[1] HIRANMAY SAHA,[1] and SANHITA MAJUMDAR [1,2]

1.—Center of Excellence for Green Energy and Sensor Systems (CEGESS), Indian Institute of Engineering Science and Technology (IIEST), Shibpur, Howrah 711103, India. 2.—e-mail: email2sm@gmail.com

Phase-pure alpha-iron-oxide (α-Fe_2O_3) nano-powders were obtained via Pechini gel-combustion using iron nitrates as an oxidant and different organic compounds (L-alanine, glycine, citric acid, oxalic acid, tartaric acid and urea) as fuels. The complex precursors isolated before the system's combustion were characterized by thermal analysis (TGA). After combustion, the as-synthesized powders were calcined at 600°C to obtain the α-Fe_2O_3 phase and eliminate the residual carbon. The powders prepared using different fuels were characterized using x-ray diffraction and field emission scanning electron microscopy. *n*-type gas sensitivity of thick film resistive sensors fabricated by using α-Fe_2O_3 powders was investigated in detail and it was observed that amongst the different fuels, citric acid-derived α-Fe_2O_3 is methane selective at 120°C operating temperature, examined in the presence of other similar types of resistive gas analyses of the same concentrations.

Key words: Alpha-Fe_2O_3, gel-combustion, fuels, nanocrystalline, gas sensor

INTRODUCTION

Hematite (α-Fe_2O_3) having corundum (α-Al_2O_3) crystal structure[1] is the most stable iron oxide under ambient conditions. Its magnetic structure shows a canted antiferromagnetic material (Neel temperature 960 K).[2–4] Moreover, α-Fe_2O_3 is an *n*-type semiconducting oxide with an optical band gap of 2.1 eV at 300 K.[3, 5]

Besides its traditional use as a red pigment in art paints and in anti-corrosion protective paints,[6] it is also used in solar cells,[3, 5] as negative electrodes in rechargeable batteries[6, 7] and as an electrochromic material.[8–10] Moreover, it has attracted enormous attention as a gas sensor material due to its good sensitivity.[11–16]

In gas sensing applications, nano-sized powders have shown outstanding properties, especially sensors made with them, which have shown low operating temperature, high sensitivity and high selectivity.[17, 18] Nano-crystalline α-Fe_2O_3 powders have been prepared through various methods such as liquid phase deposition,[11] co-precipitation,[12, 13] plasma-enhanced chemical vapor deposition,[14–16] sol-gel process[19] and laser ablation technique[20]. One of the prominent chemical synthesis routes for nano-sized powder synthesis is the solution-polymerization technique, better known as gel-combustion synthesis or the 'Pechini' method. The gel-combustion process is based on the rapid auto-ignition of a gel formed from a salt of the desired metal (e.g., nitrate, which is a strong oxidizer) and organic fuel. The parameters, which influence the reaction, include the type of the fuel, fuel to oxidizer ratio, amount of excess oxidizer, ignition temperature and water content of the precursor mixture (mixture concentration).[21, 22] Combustion-synthesized powders are generally homogeneous, having fine particle size high surface area.

(Received September 14, 2020; accepted March 6, 2021; published online March 27, 2021)

In the present study, we have synthesized nano-sized α-Fe_2O_3 powders by the gel-combustion process using different fuels (e.g., L-alanine, glycine, citric acid, oxalic acid, tartaric acid and urea). The effect of different fuels on the combustion synthesis of α-Fe_2O_3 as well as the gas sensing properties of synthesized α-Fe_2O_3 powders towards 500 ppm of methane and other similar kinds of gases (like, butane, ammonia, carbon dioxide, etc.) was studied in detail to get a selective sensor, keeping in view the importance of the methane gas which is the major constituent of natural gas. Since methane is an odorless, colorless, flammable gas, it cannot be detected by natural human organs and thus, the fabrication of a dedicated sensor is of prime importance for its safe handling.

EXPERIMENTAL

For the present study, L-alanine, glycine, citric acid, oxalic acid, tartaric acid and urea were used as fuels. Some of their properties from the literature[23–25] are listed in Table I. Firstly, 0.2 (M) ferric nitrate solution was prepared in a 500 mL beaker. 'Equivalent stoichiometric ratio' (for metal nitrates) of an organic fuel was added to the solution. Here, the stoichiometry of the redox mixture for combustion was calculated from the total oxidizing and reducing valences of the oxidizer (O) and the fuel (F), which serve as numerical coefficients so that the equivalence ratio, 'c' (O/F), becomes the unity.[26, 27]. According to propellant chemistry principles, the oxidizing and reducing valences of various elements are taken as C = 4, H = 1, O = −2, N = 0, M = 2,3,4, etc. [Here M = Fe = 3]. After adding the fuel to ferric nitrate, the mixture was heated continuously with constant stirring. The homogeneously mixed solution became viscous and turned into a gel during controlled heating, followed by self-ignition with glowing flints. Once ignited, the glowing flints slowly propagated to the entire volume of the gel. The combustion process produced CO_2, H_2O and N_2 gases; Finally, the powder was calcined at 600°C for 2 h in air to eliminate the residual carbon and obtain phase pure α-Fe_2O_3. Similarly, α-Fe_2O_3 powders were prepared using other fuels. The overall reactions between iron nitrate and different fuels are presented in Equations 1–6 separately:

$$Fe(NO_3)_3 + C_3H_7NO_2 = 1/2\alpha - Fe_2O_3 + 3CO_2 + 7/2H_2O + 2N_2 \quad (1)$$

$$Fe(NO_3)_3 + 5/3C_2H_5NO_2 = 1/2\alpha - Fe_2O_3 + 10/3CO_2 + 25/6H_2O + 7/3N_2 \quad (2)$$

$$Fe(NO_3)_3 + 5/6\,C_6H_8O_7 = 1/2\alpha - Fe_2O_3 + 5CO_2 + 10/3H_2O + 3/2N_2 \quad (3)$$

$$Fe(NO_3)_3 + 15/2\,C_2H_2O_4 = 1/2\alpha - Fe_2O_3 + 15CO_2 + 15/2H_2O + 3/2N_2 \quad (4)$$

$$Fe(NO_3)_3 + 3/2\,C_4H_6O_6 = 1/2\alpha - Fe_2O_3 + 6CO_2 + 9/2H_2O + 3/2N_2 \quad (5)$$

$$Fe(NO_3)_3 + 5/2\,CH_4N_2O = 1/2\alpha - Fe_2O_3 + 5/2CO_2 + 5H_2O + 4N_2 \quad (6)$$

Thermogravimetric analyses (TGA) of the as-synthesized powders were carried out on a Shimadzu, TA-50 instrument. The calcined powders' phase identification was carried out on an x-ray diffractometer (Rigaku Ultima IV). The powders' particle morphology was observed in a Field Emission Scanning Electron Microscope or FESEM (Carl Zeiss Microscopy Ltd, Sigma O2-87) after ultrasonically dispersing the powder in acetone.

Table I. Some relevant properties of organic compounds used in this study

Properties	Organic compounds					
	L-Alanine	**Glycine**	**Citric acid**	**Oxalic acid**	**Tartaric acid**	**Urea**
Formula	$C_3H_7NO_2$	$C_2H_5NO_2$	$C_6H_8O_7$	$C_2H_2O_4$	$C_4H_6O_6$	CH_4N_2O
Molecular weight (g/mol)	89.09	75.07	192.1	90	150	60.1
$\Delta H_{(C)}^{\circ}$ * (kJ/mol)	1576.9	973.1	1959.4	251.1	1149.9	631.6
Moles of gases for 1 mole α-Fe_2O_3	8.5	9.83	9.83	24	12	11.5
Decomposition temperature (°C)	314	262	175	101	170	135

$\Delta H_{(C)}^{\circ}$: Enthalpy of combustion of organic compounds for solid state.

For fabricating sensors from the synthesized powders, thick pastes of the powder were prepared in an aqueous medium containing a small amount (3 wt.%) of the PVA (polyvinyl alcohol) binder. The suspension has been drop coated on a thermally oxidized Si wafer (where the thickness of Si and SiO_2 are $\sim 180\ \mu m$ and ~ 300 nm, respectively) having a dimension of 7 mm 3 mm (substrate resistivity 1–2 Ωcm; <100> CZ). On the topside, aluminum (Al) electrodes were deposited by thermal evaporation (HHV AUTO 500; vacuum pressure of $\sim$ 10-5 bar, deposition rate 3 nm/s,) having 100 nm thickness and using a suitably designed metal shadow mask. Figure 1 illustrates the sensing set-up for better understanding. The figure describes step-by-step the powder formation process of α-Fe_2O_3 and measurement of sensing properties using an in-house indigenous sensor set-up. Drop in resistance was observed after exposure to the analyte gas(es) (reducing type). This change in resistance was recorded using Keysight precision source meter [B2901A] at room temperature as well as at elevated temperatures, in presence of ambient humidity of $\sim$ 60% to 65%. The real images of fabricated sensors and sensing set-up are also incorporated in the scheme. The sensors were initially aged at 100°C for seven days to achieve the desired stability before the measurements.

RESULTS AND DISCUSSION

Thermal Gravimetric Analyses of the Precursors

Figure 2 shows the typical thermogravimetric analyses (TGA) curves of the various precursors prepared using different organic fuels. TGA plotsrecord the weight loss of materials at different temperatures and help us get an idea about the synthesized material's probable calcination temperature. The curves imply the temperature versus the weight-loss percentage of the as-prepared materials up to 1000°C, but it can be seen that almost all powder precursors cease their weight reduction after 600°C, predicting their probable calcination temperature at 600°C. All powders, though derived from different organic fuels, show similar types of emaciation (single step). They all show a significant weight loss (80%) around 400°C temperature, indicating that the significant chemical reactions took place very rapidly within this temperature range leading to the arrangements of the atoms in iron oxy-hydroxides that, in turn, lead to the consolidation of the iron-oxide structure and its crystallization process. The phenomena are supported by the slope of weight loss versus temperature curves, which are very steep. Table II depicts the temperature of each combustion reaction's initiation and the physical properties of synthesized α-Fe_2O_3 after

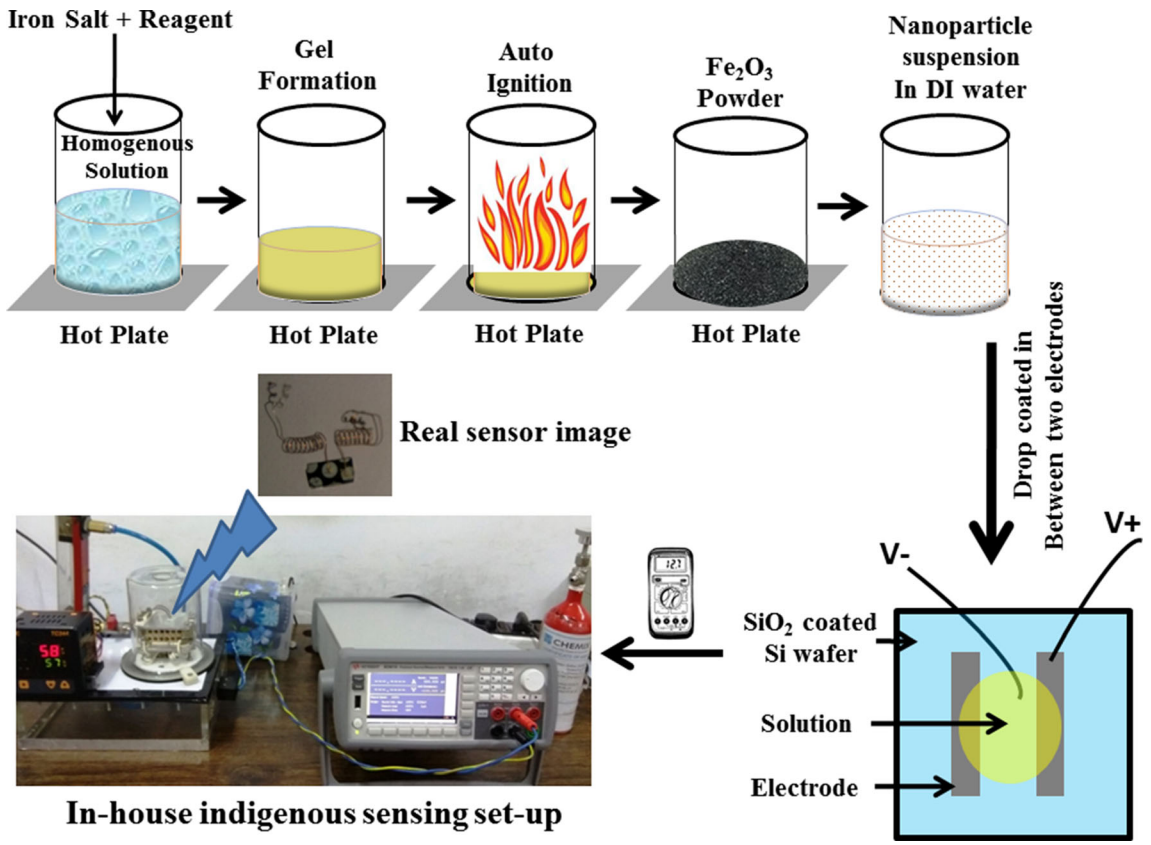

Fig. 1. Schematic representation of power preparation and sensing measurement in the sensing set-up.

calcination of the ash at 600°C. From this table, one may perceive the effects of various organic fuels (like L-alanine, glycine, citric acid, oxalic acid, tartaric acid, urea) on the reaction temperature and physical properties of synthesized α-Fe_2O_3. Physical properties like initiation temperature (the temperature when the sample weight goes down rapidly due to combustion), the crystallite size (calculated from the line broadening of the (110) XRD peak using the Scherrer formula), particle size (calculated from the FESEM micrographs using 'Image J' software) and surface area (calculated from N_2 adsorption-desorption experiments using BET method) of α-Fe_2O_3 synthesized following similar method and reaction conditions, may vary widely due to variation in fuel to ferric nitrate ratio. Since sensing is all about surface phenomena, it can be easily understood that increased surface area as well as reduced particle size and crystallite size boosted the probability of sensitivity. From Table II, it can be seen that citric acid derived α-Fe_2O_3 has the maximum surface area and minimum particle size and crystallite size, followed by L-Alanine, Oxalic acid, etc. It has been observed that sensing trends also follow a similar pattern.

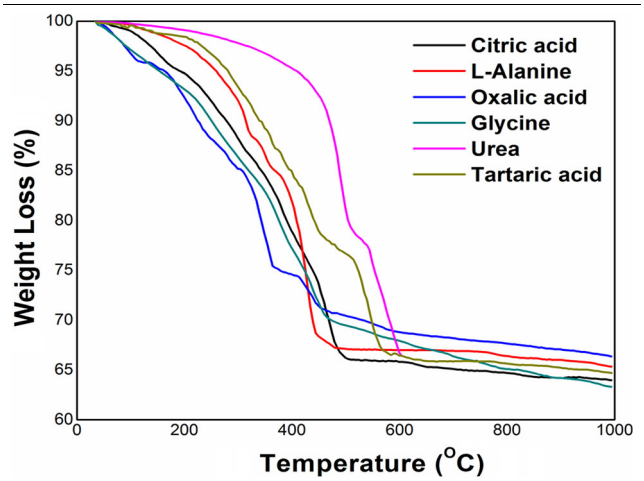

Fig. 2. Thermogravimetric analyses of α-Fe_2O_3 powders derived from different fuels (viz., L-alanine, glycine, citric acid, oxalic acid, tartaric acid and urea).

Phase Analyses of the Products

Figure 3 shows the XRD patterns of α-Fe_2O_3 powders, indexing the Miller indices (*hkl*) of the reflecting planes, after calcination of the ashes at 600°C for 2h. The XRD patterns of the synthesized powders matched well with the reported reference pattern of polycrystalline Fe_2O_3 (standard hematite, JCPDS card no.: 33-0664; representative reflections of the same have been presented in Fig. 3 at the bottom-most). The mean crystallite size of the powder was calculated using the Scherrer formula[28]

$$D = 0.9\lambda/\beta\cos q, \tag{7}$$

where '*D*' is the average crystallite size, l = 1.541 Å (x-ray wavelength) and $\beta = \sqrt{(B^2 - b^2)}$, '*B*' being the width of the diffraction peak at half maximum for the diffraction angle two thetas and '*b*' is the same for very large crystallites. The value of 'b' was determined from the XRD of the large-grained sample prepared by calcining the powder at a high temperature. Table II shows that the crystallite sizes of the calcined powders are roughly in the range of 20–85 nm.

Microstructural Analyses

Figure 4a, b, c, d, e and f shows the typical field emission scanning electron micrographs (FESEM) of the synthesized powders (after grinding for ~10 min. in a mortar and pestle to break the soft agglomerates). The particles were dispersed ultrasonically in acetone for a reasonable period. The morphologies of the synthesized powders were visualized on a FESEM (SIGMA ZEISS) at 3 kV electron high tension (ETH) using an InLens detector having a working distance (WD) in the range of 5.4–5.9 mm. However, in this technique, samples can potentially sublimate under high vacuum conditions, thus increasing the risk of charging. To

Table II. Effects of various fuels on the reaction temperature and physical properties of synthesized α-Fe_2O_3

Fuels	Initiation temperature (°C)	Crystallite size[b] (nm)	Particle size[c] (nm)	Surface area[d] (m^2/g)
L-Alanine	161	50.2	55	15.4
Glycine	165	63.0	70	11.7
Citric acid	143	22.8	25	45.5
Oxalic acid	169	48.5	50	12.2
Tartaric acid	225	72.7	75	9.3
Urea	215	85.4	90	5.9

[a]Initiation temperature (T_{in}): a temperature when the sample weight goes down rapidly due to combustion.
[b]Crystallite size of the as-synthesized α-Fe_2O_3 powders calculated from the line broadening of the (110) XRD peak using Scherrer formula.
[c]Particle size of the α-Fe_2O_3 powders calculated from the FESEM micrographs using 'image J' software (v-1.6.0).
[d]Surface area of the α-Fe_2O_3 powders calculated from N_2 adsorption-desorption experiments using BET method.

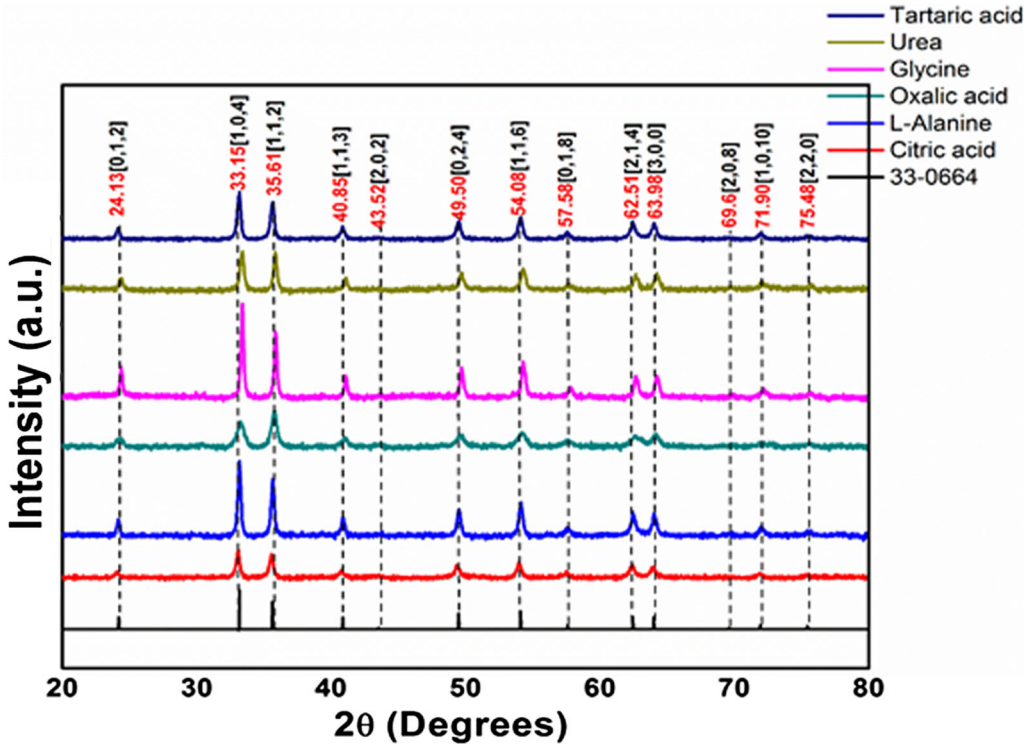

Fig. 3. X-ray diffractogram patterns of α-Fe_2O_3, derived from different fuels (viz., L-alanine, glycine, citric acid, oxalic acid, tartaric acid and urea) along with the representative reflections of α-Fe_2O_3 in JCPDF file no.: 33-0664.

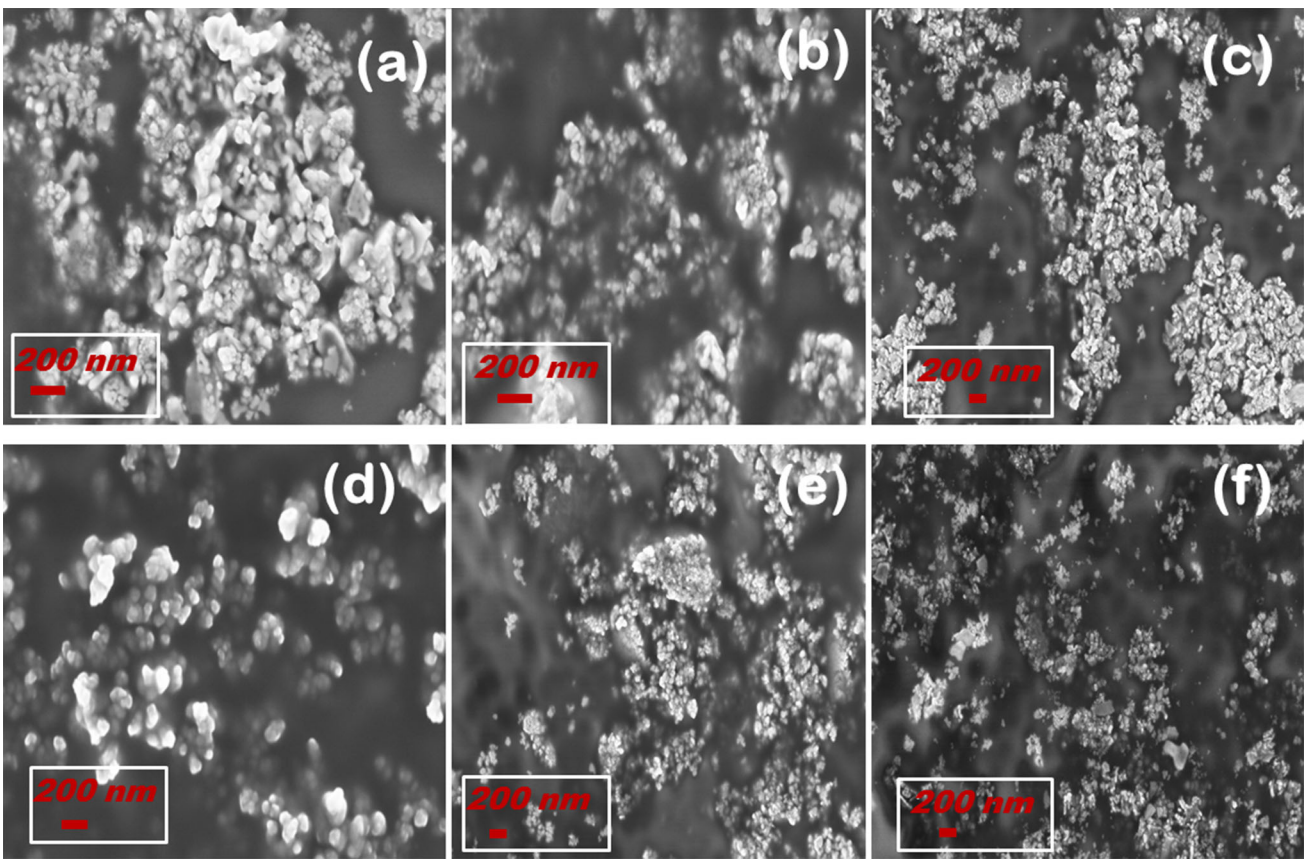

Fig. 4. FESEM micrographs of α-Fe_2O_3 derived from six different fuels [viz., (a) urea, (b) L-alanine, (c) glycine, (d) citric acid, (e) tartaric acid and (f) oxalic acid] with same (200 nm) bar indicator.

restrict this tendency, an aluminum (Al) foil tape was attached with each sample stage for discharging, if necessary. The images showed that the powders are mostly agglomerated, though the degree of agglomeration varies from precursor to precursor. Citric acid derived powder (Fig. 4d) showed the least agglomeration amongst the bunch. The morphologies can be attributed to the liberation of many gases during combustion reaction, indicating favorable morphologies to exhibit good adsorption ability during sensing reactions.

Gas Sensing Properties

The percent response (sensitivity; $\%S$) of the sensors fabricated using the synthesized α-Fe_2O_3 powder was calculated from the following relation:[29]

$$(\%)S = [(R_A - R_G)/R_A] \times 100, \quad (8)$$

where 'R_A' is the sensor resistance in air at a particular temperature and 'R_G' is the sensor resistance in the presence of gas at the same temperature.

Figure 5 indicates the dynamic response-recovery characteristics of α-Fe_2O_3 based sensors derived from different organic fuel precursors (*viz*., L-alanine, glycine, citric acid, oxalic acid, tartaric acid and urea). The response natures are sharp in each case, indicating a short response time of the sensors, though the recovery patterns vary from sensor to sensor. The best response nature (including recovery) was exhibited by the sensor synthesized from the citric acid precursor and the worst one was presented by the sensor derived from glycine precursor.For comparison, the sensing performances of the synthesized material (α-Fe_2O_3) of previously reported works have been explored and represented in Table III, where their sensing range, detection limit and repeatability were examined.[30–36] From the table it can be observed that Hematite (α-Fe_2O_3) can be synthesized through different techniques, and, based on their preparation, various gases may be detected qualitatively and quantitatively by exploiting this material. Based on the response-recovery characteristics of Fig. 5, the sensors derived from the citric acid (black colored) have been chosen as the best ones of the bunch and have been used in further sensing studies. In this study, diverse experiments have been carried out to measure the sensitivity as a function of time. In all the cases, sensitivity showed approximately constant values, indicating the repeatability of the sensors.

Figure 6 displays the different gas sensing characteristics of α-Fe_2O_3 sensors derived from citric acid organic fuel. Figure 6a shows the percent response (%S) of α-Fe_2O_3 sensors measured at different operating temperatures, ranging between room temperature (30°C) and 150°C (with ± 2 error bar, indicating tolerance levels of %S, measured in different dates at different times).

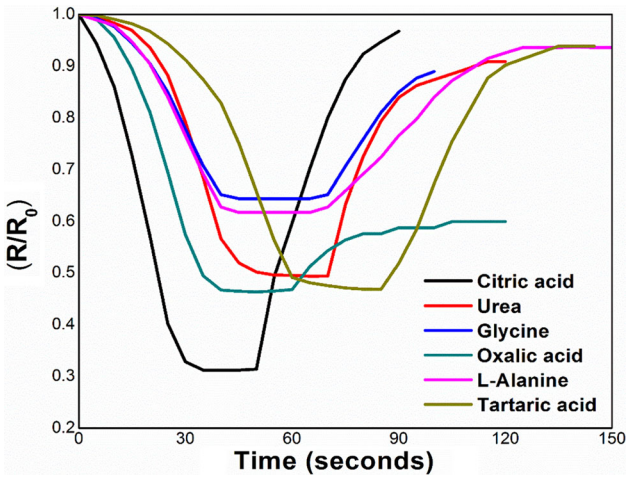

Fig. 5. Dynamic response-recovery characteristics of α-Fe_2O_3 based sensors derived from different organic fuel precursors.

It was found that the maximum response in 500 ppm n-butane was obtained at around 120°C operating temperature (peak), after which the response nature drops down (bell natured curve). Figure 6b exhibits the cross-sensitivity (selectivity) of α-Fe_2O_3 sensors, measured against different gases (viz. methane, ammonia, butane and CO_2, each having 500 ppm concentration) examined at 120°C operating temperature (with ±5 error bar). The survey indicates the methane selectivity of the synthesized material at that particular operating temperature.

Though the lower explosive limit (LEL) of methane (CH_4) is 5% by volume in air, we have chosen the gas concentration as 500 ppm, which is much lower than the flammability limit of the target gas, since we want to detect the gas before its ignition.[37] Moreover, here in this study, the synthesized sensor's operating temperature is comparatively much lower than the usual operating temperatures of the transition metal oxides-based sensors. Therefore, the optimum working temperature and the detection limit are in good accordance with each other to safely handle a flammable gas like methane (which is the principal constituent of compressed natural gas, CNG).

To understand the typical gas sensing behavior of α-Fe_2O_3, we have to consider an alkane C_nH_{2n+2} which is adsorbed (also desorbed depending on the operating temperature) on the sensor surface as given below:

$$C_nH_{2n+2}(\text{gas}) \Leftrightarrow C_nH_{2n+2}(\text{physisorbed}). \quad (9)$$

Though the final oxidation products of alkanes are CO_2, CO and H_2O, the reactions may proceed through intermediate steps,[38] e.g., decomposition of butane (one of the analyte gases, which has been examined during cross-sensitivity) may proceed via the formation of butyl, acetyl, formate, etc. groups.

Table III. Exploration of differently synthesized α-Fe_2O_3 based gas sensors for their sensing range, detection limit and repeatability

Sl. No.	Routes of synthesis	Sensing range	Detection limit and repeatability	References
1.	Homogeneous co-precipitation method	0–4000 ppm methane conc.	The maximum response was observed for 2000 ppm CH_4 at room temperature. There are no data about repeatability.	30
2.	Co-precipitation method	20–80 ppm methyl mercaptan conc.	The synthesized material exhibits 72% sensitivity against 80 ppm CH_3SH at room temperature. The sensors showed a direct dependence with the concentrations in the range from 20 to 80 ppm at room temperature, with very good reproducibility	31
3.	Nano-casting method	Ethanol gas concentration from 50 ppm to 2000 ppm on the sensitivity at 280°C have been discussed	At 280°C, the synthesized sensors exhibited 45.56% highest sensitivity against 100 ppm ethanol gas. Samples showed excellent long-term stability and repeatability with a negligible variation	32
4.	Hydrothermal route	1–5 ppm NO_2 concentration	At 200°C the sensor response presents a maximum value of 3.4 for 5 ppm of NO_2. The sensor confirms the reproducibility and repeatability even after one month time period	33
5.	Porous quasi-single crystal hierarchical tubule was fabricated by using poplar branch as a confined micro-reactor	58.6 ppb to 34.9 ppm H_2S gas concentrations	The fabricated sensor with a short response time has higher sensitivity of 24.3–10 ppm H_2S at a low working temperature of 133°C. After 5 cycles of response, the gas sensor maintains the initial response, indicating satisfactory repeatability	34
6.	Vertical foating catalyst chemical vapor deposition (FC-CVD) process	LPG concentrations varying from 0.1 to 0.7 vol.%.	The sensing performance showed that it could detect LPG concentration at a lower value than 25% of LEL with a response/recovery time of less than 30 s at room temperature. It is observed that the sensor response was stable and nearly equal at each concentration, indicating good reproducibility of the sensing performances	35
7.	Ultrafine nanoparticles were prepared by a reverse microemulsion method	Acetone concentrations from 5 ppm to 3000 ppm were examined at a working temperature of 340°C	The highest response against 3000 ppm acetone was 36% at 340°C temperature. The sensors reported good stability though the repeatability data are absent	36

The response of the sensors goes down drastically above 120°C. Such behavior can be understood by considering the role of desorption of gas molecules (Eq. 9) at higher temperatures.

Incidentally, transition metal oxides like Fe_2O_3 are primarily used as redox catalysts and their acid-base properties are also of significant importance.[39] In α-Fe_2O_3, Lewis acid sites (Fe^{+3}) are the active

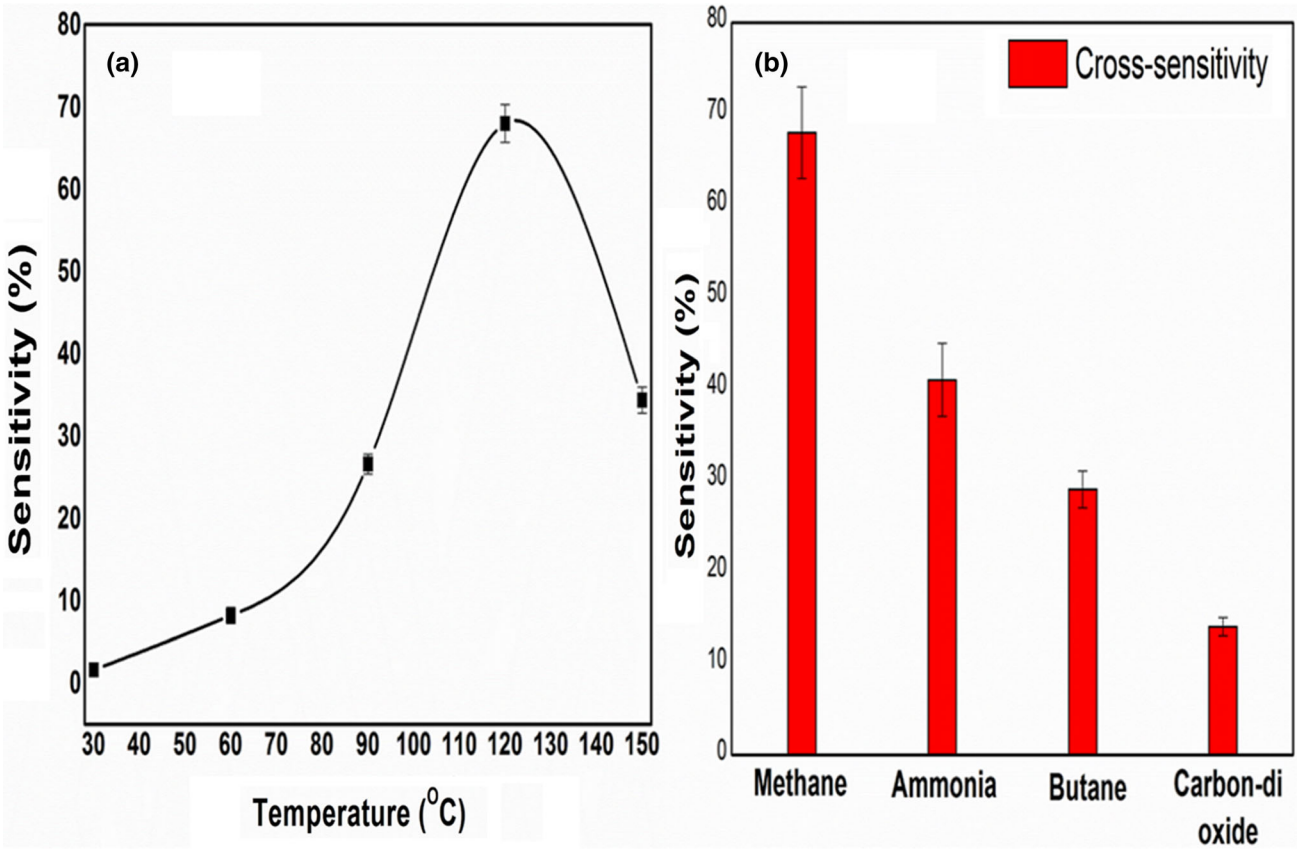

Fig. 6. (a) Variation of percent sensitivity to operating temperature, measured against methane gas of 500 ppm and (b) cross-sensitivity (selectivity) measured against different gases (*viz.* methane, ammonia, butane and CO_2, each of 500 ppm concentration) at 120°C operating temperature

positions where adsorption or oxidation occurs. The conversion and selectivity of a particular reaction are influenced not only by the nature of the active sites but also by their number, strength, and size.[40–42] Here, the enhancement of the gas sensing performance for combustion-synthesized α-Fe_2O_3 using citric acid as a fuel may be attributed to the increase in the number of active sites. However, further work is needed to determine the nature and concentration of active sites present on α-Fe_2O_3 powders prepared using different fuels.

CONCLUSION

Phase pure α-Fe_2O_3 nano-powders were obtained by the gel-combustion Pechini method using iron nitrate as an oxidant and different organic compounds as fuels (L-alanine, glycine, citric acid, oxalic acid, tartaric acid, and urea). The effects of fuel type on the synthesized powders' physical properties and their response towards different reducing gases like methane, butane, ammonia, and carbon-di-oxide were investigated. It was observed that amongst the different fuels, citric acid derived α-Fe_2O_3 showed good sensitivity and selectivity towards methane (the main constituent of CNG). The maximum response was recorded against methane at 120°C operating temperature in the presence of other similar reducing gases of the same concentration, indicating its methane selectivity at that particular temperature. Similar approaches for synthesizing and processing to achieve desired physical properties like crystallite and particle size, morphology, particle size distribution, surface area, etc. for optimizing sensing properties for a particular target gas (like methane) may be beneficial for other transition metal oxides-based gas sensing/monitoring systems.

ACKNOWLEDGMENTS

The authors acknowledge the characterization supports received from CSIR-CGCRI, Kolkata. S. Majumdar acknowledges the financial support received from DST WOS-A (KIRAN) [Sanction Oder No.: SR/WOS-A/CS-1054/2015]. H. Saha and A. Nandi is indebted to the Department of Science and Technology, Govt. of India for their financial support [Sanction Oder No.: DST/TMD/SERI/HUB/2(C)].

CONFLICT OF INTEREST

On behalf of all authors, the corresponding author states that there is no conflict of interest.

REFERENCES

1. M. Fuller, Experimental methods in rock magnetism and paleomagnetism, *Methods in Experimental Physics*, Vol. 470. ed. C.G. Sammis, and T.L. Henyey (Cambridge: Academic Press, 1987).
2. H.M. Lu, and X.K. Meng, *J. Phys. Chem. C* 114, 21291 (2010).
3. C.G. Shull, W.A. Strauser, and O.E. Wollan, *Phys. Rev.* 83, 333 (1951).
4. C. Leighton, A. Hoffmann, M.R. Fitzsimmons, J. Nogues, and I.K. Schuller, *Phil. Mag. B* 81, 1927 (2001).
5. P. Chauhan, S. Annapoomi, and S.K. Trikha, *Bull. Mater. Sci.* 21, 381 (1998).
6. Q. Zhang, R. Zheng, J. Ding, P. Cui, Z. Wang, P. Lv, and W. Wei, *J. Am. Ceram. Soc.* (2021). https://doi.org/10.1111/jace.17672.
7. R.C. Massé, C. Liu, Y. Li, L. Mai, and G. Cao, *Natl. Sci. Rev.* 4, 26 (2017).
8. B. Ouertani, G. Bidouk, R. Ouertani, B. Teys, and H. Ezzaouia, *Mater. Chem. Phys.* 242, 122272 (2020).
9. J.H. Kennedy, and D.J. Dunnwald, *Electrochem. Soc.* 130, 2013 (1983).
10. J. Sarradin, M. Ribes, A. Guessous, and K. Elkacemi, *Solid State Ionics* 112, 35 (1998).
11. G. Neri, A. Bonavita, S. Ipsale, G. Rizzo, C. Baratto, G. Faglia, and G. Sberveglieri, *Maters. Sc. Engg. B* 139, 41 (2007).
12. J.S. Han, T. Bredow, D.E. Davey, A.B. Yu, and D.E. Mulcahy, *Sens. Actuators B* 75, 18 (2001).
13. N.T.A. Thu et al., *Sens. Actuators B* 255, 3275 (2018).
14. E.T. Lee, G.E. Jang, C.K. Kim, and D.H. Yoon, *Sens. Actuators B* 77, 221 (2001).
15. H.-J. Zhang, F.-N. Meng, L.-Z. Liu, and Y.-J. Chen, *J. Alloys Comp.* 774, 1181 (2019).
16. Y. Cheng, H. Guo, Y. Wang, Y. Zhao, Y. Li, L. Liu, H. Li, and H. Duan, *Mater. Res. Bull.* 105, 21 (2018).
17. S. Majumdar, A. Nandi, and H. Saha, *IEEE Sens. J.* 18, 6517 (2018).
18. A. Nandi, P. Nag, D. Panda, S. Dhar, S.M. Hossain, H. Saha, and S. Majumdar, *ACS Omega* 4, 11053 (2019).
19. X.Q. Liu, S.W. Tao, and Y.S. Shen, *Sens. Actuators B* 40, 161 (1997).
20. Y. Nakatani, and M. Matsuoka, *Jpn. J. Appl. Phys.* 21, 1758 (1982).
21. S.R. Jain, K.C. Adiga, and V.R. Pai Verneker, *Comb. Flame* 40, 71 (1981).
22. M.P. Pechini, US Patent 3,330,697 (1967).
23. W.M. Haynes (Edt.) CRC Handbook of Chemistry and Physics, 95th Edn. CRC press LLC, New York, 5-82-91 (2014-15).
24. R.H. Perry, and C.H. Chilton, *Chemical Engineering Handbook*, 7th ed., (New York: McGraw-Hill, 1997).
25. J.A. Dean, *Lange'sHandbook of Chemistry*, 15th ed., (New York: McGraw-Hill, 1998).
26. L.E. Shea, J. Mckittrick, and O.A. Lopez, *J. Am. Ceram. Soc.* 79, 3257 (1996).
27. S.R. Jain, K.C. Adiga, and V.R. Paivernekar, *Combust. Flame* 40, 71 (1981).
28. S. Majumdar, *Ceram. Int.* 41, 14350 (2015).
29. S. Majumdar, *Appl. Surf. Sci.* 376, 290 (2016).
30. H. Liu, T. Peng, H. Sun, R. Xie, and G. Ma, *RSC Adv.* 7, 11414 (2017).
31. D. Garcia, G. Picasso, P. Hidalgo, H.E.M. Peres, R.S. Kou, and J.M. Goncalves, *Anal. Chem. Res.* 12, 74 (2017).
32. J.N. Mao, B. Hong, H.D. Chen, M.H. Gao, J.C. Xu, Y.B. Han, Y.T. Yang, H.X. Jin, D.F. Jin, X.L. Peng, J. Li, H.L. Ge, and X.Q. Wang, *J. Alloys Comp.* 827, 154248 (2020).
33. M. Hjiri, M.S. Aida, and G. Neri, *Sensors* 19, 167 (2019).
34. Y. Teng, X.-F. Zhang, T.-T. Xu, Z.-P. Deng, Y.-M. Xu, L.-H. Huo, and S. Gao, *Chem. Eng. J.* 392, 123679 (2020).
35. B. Chaitongrat and S. Chaisitsak, 2018, 9236450 (2018).
36. S. Liang, J. Li, F. Wang, J. Qin, X. Laib, and X. Jiang, *Sens. Actuators B* 238, 923 (2017).
37. H. Ma, Y. Du, M. Wei, E. Ding, and L. Lin, *Sens. Actuators A* 295, 70 (2019).
38. D. Kohl, *J. Phys. D: Appl. Phys.* 34, R125 (2001).
39. S. Mustafa, S. Tasleem, and A. Naeem, *J. Colloid Inter. Sci.* 275, 523 (2004).
40. A. Auroux, and A. Gervasini, *J. Phys. Chem.* 94, 6371 (1990).
41. N. Lopez, T.V.W. Janssens, B.S. Clausen, Y. Xu, M. Mavrikakis, T. Bligaard, and J.K. Nerskov, *J. Catal.* 223, 232 (2004).
42. P. Li, D.E. Miser, S. Rabiei, R.T. Yadav, and M.R. Hajaligol, *Appl. Catal. B* 43, 151 (2003).